Journal of African Earth Sciences 150 (2019) 441–450

Contents lists available at ScienceDirect

Journal of African Earth Sciences

journal homepage: www.elsevier.com/locate/jafrearsci

Strain analysis and deformation history of Zalm area, Arabian shield, Saudi Arabia

Ali Y. Kahal[a], Essam Abd El-Motaal[a,b], Osama M.K. Kassem[a,c,*], Abed H.R. Al Ghoreiby[a]

[a] SGSRC, Department of Geology, College of Science, King Saud University, P.O. Box 2455, Riyadh, 11451, Saudi Arabia
[b] Geology Department, Faulty of Science, Al-Azahr University, Nasr City, Cairo, Egypt
[c] Geology Department, National Research Center, Al-Behoos Str., 12622, Dokki, Cairo, Egypt

ARTICLE INFO

Keywords:
Finite strain
Neoproterozoic
Deformation
Western Arabian shield
Zalm
Saudi Arabia

ABSTRACT

The present work deals with the strain analysis and deformation of the Zalm area which is located in the central part of the central Nabitah suture belt, which separates the continental Afif terrane from the ensimatic arc terranes of the western Arabian Shield. This study carried out through field investigation, strain parameters, and microscopic examination for understanding the nature of deformation in the Zalm area. On the basis of the field investigation and the geometry of the contact, it is more likely that the contact between ultramafic rocks and gabbroic rock complex is low-angle thrust faulting. The granitoid rocks are divided into the quartz monzodiorite, monzogranite, alkali-feldspar granite and leucocratic-granodiorite. The R_f/ϕ and Fry techniques on feldspar and mafic grains from 53 samples representative of each rock type were collected in the field. Strain data shows that the deformation of the granitic, metavolcanic and amphibole schist samples range from high to moderate. The axial ratios (XZ section) range from 1.60 to 4.10 for the R_f/ϕ method and 2.80 to 4.90 for the Fry method. Furthermore, the finite strain data does not dispay any significant difference in the deformation behavior between Rf/ϕ and Fry methods. We concluded that the strain magnitude has the same order of deformation in the deformed granitoid and amphibole schist rocks. The majority of samples are in a zone of flattening symmetry, while a few samples are showing constrictional symmetry. In addition, it is noted that the short axes (Z) are sub-perpendicular related with a sub-parallel foliation. Furthermore, the nappe contact are designed during the intrusion of plutons associated with faults in the Zalm regions under brittle to semi-ductile deformation conditions.

1. Introduction

The Arabian Shield displays amalgamated tectonostratigraphic (e.g. Midyan, Hijaz, Asir, Afif, and Ar Rayn) terranes of Tonian (1000–850 Ma) and Cryogenian (850–650 Ma) volcanic and plutonic rocks (Johnson et al., 2003, 2011; Johnson and Kattan, 2012). This led to the formation of a 40–100 km thick lithosphere of the Arabian Shield (Mooney et al., 1985; Altherr et al., 1990; Camp and Roobol, 1992; Sandvol et al., 1998; Hansen et al., 2007). The terranes are separated by four orogenic (e.g. Yanbu, Bir Umq, Nabitah, and Al Amar) suture zones. North and northeast trending of the sutures are assumed between the distinct terranes on the basis of ophiolite- and serpentinite-decorated shear zones (Al-Shanti and Mitchell, 1976; Johnson et al., 2004). NE-oriented Yanbu suture is situated between the Midyan and Hijaz terranes in the northwestern side of the Arabian Shield (Fig. 1). The ophiolites of the Arabian Shield range in age from ~690 to ~870 Ma, and have a mean age of ~780 Ma that may approximate the onset of terrane accretion (Stern et al., 2004).

The Zalm area is situated between Lat. 22° 30′ and 23° 00′ N and Long. 42° 00′ and 42° 30′ E (Fig. 1). It is located in the Nabitah suture zone, which separates Afif terrane from the ensimatic arc terranes of the western Arabian Shield. Also, the Zalm area is located in the central part of the central Nabitah suture belt, which is characterized by the predominance of the N—S and NW-SE structural trends. The major NW-oriented faults are related to the Najd Fault System, which represents the latest tectonic event that affected the Arabian Shield during the Pan-African tectono-thermal orogeny. The study area is generally of low relief. The mountainous area is isolated in the northern part, and the highest relief is Jabal Zalm which rises about 300 m above the surrounding plains and 1150 m above the sea level. Wadis generally run from south to north. The drainage pattern system is dendritic particularly around Jabal Zalm.

* Corresponding author. SGSRC, Department of Geology, College of Science, King Saud University, P.O. Box 2455, Riyadh, 11451, Saudi Arabia.
E-mail address: kassemo1@yahoo.com (O.M.K. Kassem).

https://doi.org/10.1016/j.jafrearsci.2018.09.008
Received 2 March 2018; Received in revised form 18 July 2018; Accepted 13 September 2018
Available online 25 September 2018
1464-343X/

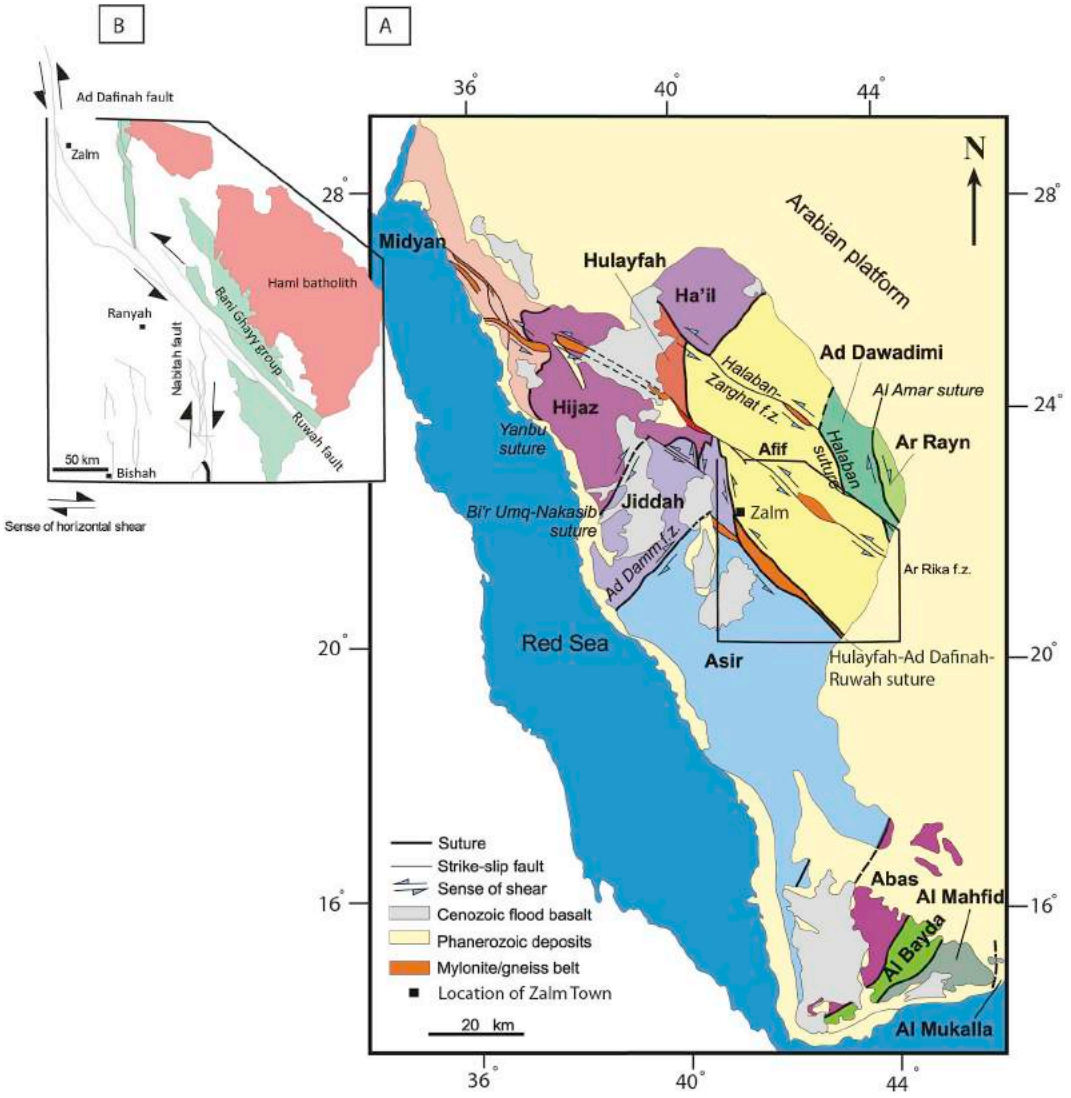

Fig. 1. A) Tectonostratigraphic terranes in the Arabian Shield (modified after Stoeser and Camp, 1985 and Johnson et al., 2003) B) Structural map of Zalm region and adjacent area.

The finite strain analysis investigate the natural of shear zones which display oblate geometries (Coward, 1976; O´Hara and Blockburn, 1989; Ring, 1999; Kassem and Ring, 2004; Kassem, 2012 & 2015). Many authors suggested that the oblate fabrics formed during the volume loss in simple shear zones or during shearing in pure shear with or without volume loss (Simpson and De Poar, 1993; Mukul and Mitra, 1998; Kassem and Abd El Rahim, 2010; Kassem et al., 2012). It is important to quantify the strain analysis and the degree of non-coaxiality. Furthermore, the evaluation of strain shapes and the relation of the flatting foliations are characteristic of nappes in the internides of many regions. The contacts are shown major lithological boundaries in the Arabian shield and the occurrence of granitic, metavolcanic and amphibole schist rocks are used to show nappe boundaries (Fritz et al., 1996; Neumayr et al., 1996, 1998). In the Zalm area, it is necessary to investigate the contact between the different units such as granitic, metavolcanic and amphibole schist rocks. In addition, a major lithological margin display the trace of a low angle thrust fault (Stern, 1985).

This study was realized through field observation, finite strain and microscopic study to quantify the tectonic evaluation in the Zalm area. The microstructural and petrological investigations are important to display the characterization of the nappe contacts suggesting that deformation history was applied to the existing nappe structure. Furthermore, the present work will depend on our structural data to explain strain symmetry in the Zalm area (Kassem, 2011 &, 2014; Kassem et al., 2016).

2. Geological setting

The Zalm area is mostly made up of Neoproterozoic ultramafic-mafic rock complexes intruded by granitoid plutons. It displays older Cryogenian layered rocks (Tamran Formation and Siham Group) and younger Cryogenian intrusive plutons (Jidh Suite and Humaymh Suite) (Fig. 2). Tamran formation covers the northwestern part of the study area, and is made up of metamorphosed pyroclastic and volcanoclastic rocks and bounded to the east by ultramafic rocks and intruded by monzogranite.

The volcano-sedimentary sequence of the Siham Group is made up of basalt, rhyolite, andesite, shale, lithic sandstone, conglomerate, marble and quartzite. The variation in amounts and thicknesses of these rocks is interpreted in the cross-section and reflected from deep water in the west to a shallow continental margin in the east. The Siham Group is considered as a volcanoclastic rocks in the east dipping associated with subduction zone in the eastward shallowing basin. It grades from oceanic and volcanic to continental-margin and sedimentary from west to the east. The Siham Group in the study area is observed around Zalm village and mainly consists of mafic to intermediate flows, marble,

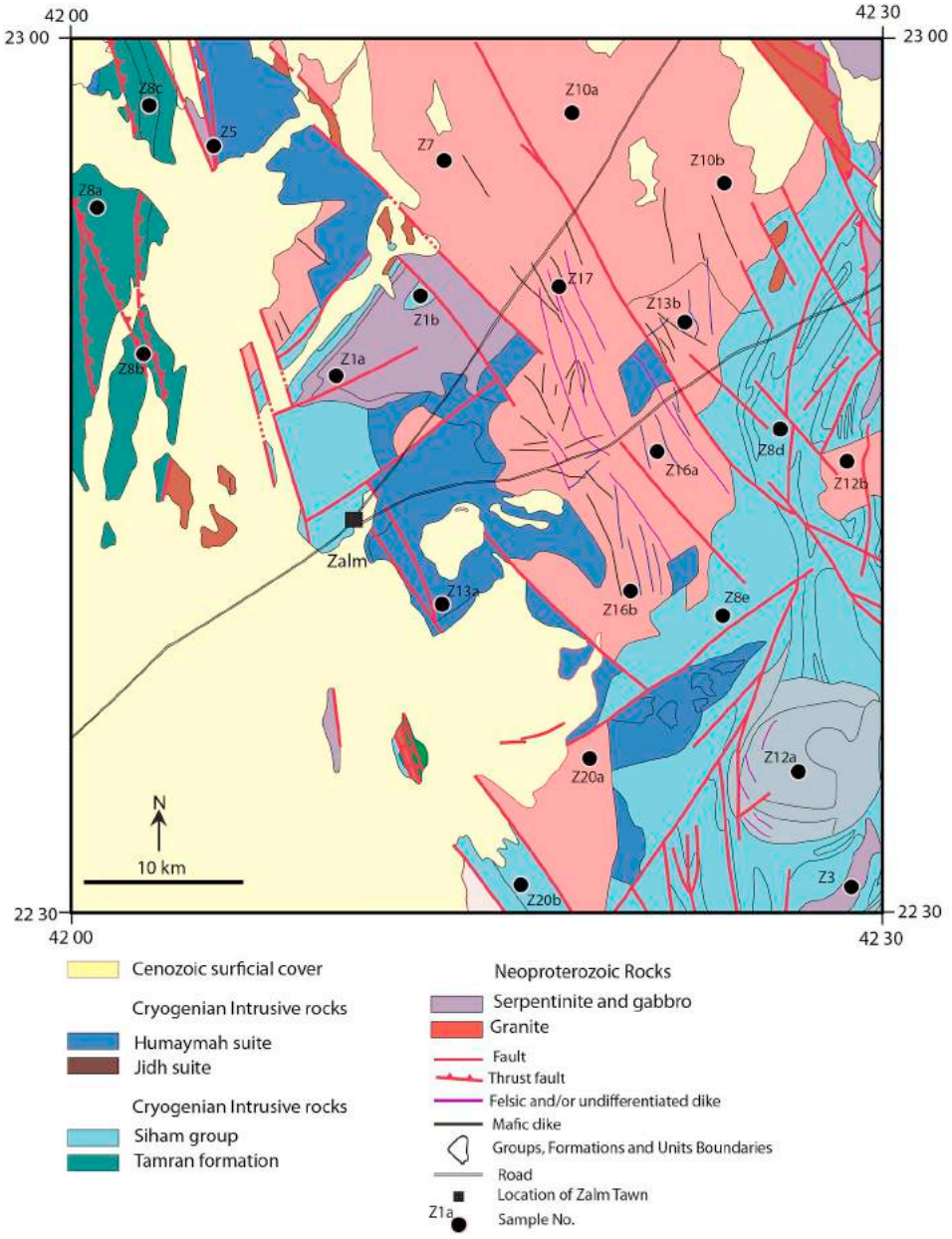

Fig. 2. Geologic map of the Zalm area and samples locations.

and subordinate silicic pyroclastic rocks (Fig. 2). The different lithology of Siham Group are mostly weakly to moderately deformed, however they are locally schistose faces and caught up in thrusting. The Neoproterozoic ultramafic units contain serpentinite and gabbro which represented the ophiolites of the Zalm area. They are also well-preserved as slices of mafic-ultramafic rock along shear zones, and gneiss and schist rocks created from protoliths along shear zones. The Zalm ultramafic complex is exposed as a 20 km long and about 7 km wide belt trending northern east. The Zalm area is bounded by layered gabbro to the south and by post-orogenic granite intrusions to the southeast, east, and northeast. It forms a segment of the larger Ad-Dafinah belt which is considerable a part of the Nabitah suture zone. The ultramafic rocks form both Jabal Zalm and also exposed as scattered bodies in the eastern reaches of the study area. On the basis of the field investigation and the geometry of the contact, it is more likely that the contact between ultramafic rocks and gabbroic rock complex are low-angle thrust faults. The ultramafic rocks are intensively affected by a NE-oriented shear zone in the northeastern part of the area, where they are altered to talc carbonate, leaving nuclei of peridotite serpentinite relics. Gold-bearing quartz veins crosscut the serpentinites along N40 to 60° trends. These veins have been mined by ancient workings.

Gabbroic rock complex (Humaymah suite) occurs as flat or low-lying hills with a distinctive blocky and massive appearance in the central part of the study area (Fig. 2). They are dark-green to greenish-black in color. The gabbroic rocks have been identified by two types within the study area: the first type is an uralite meta-gabbro, and the second type is a hornblende gabbro. In some locations, these gabbroic rocks are strongly sheared with the development of foliation trending N45°E and dipping 70° southeast. The gabbroic rocks are dissected by veinlet-developed microfractures filled by carbonates, quartz, and epidote, where minor-scale faults dislocate these veinlets. The gabbro, close to the contact with the ultramafic rocks, is characterized by rhythmic layering.

The Jidh suite is represented by calc-alkalic intrusive rocks emplaced in the Siham group in the west-central part of the Afif terrane. The age dating of rocks are not measured, on the other hand, in the Siham group, the main deformation event are predated as structural

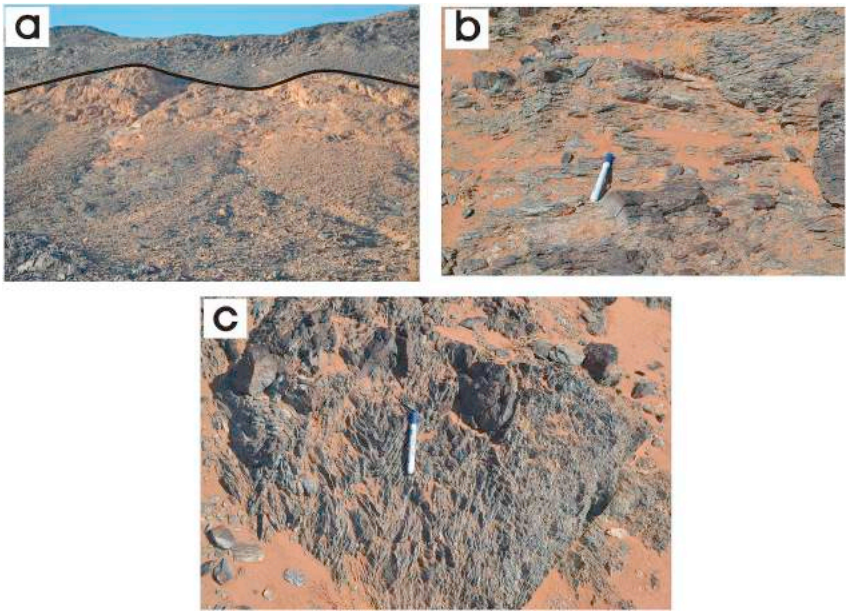

Fig. 3. (a) Field photograph showing the contact between amphibolite schist and shared granite. (b) Field photograph showing the foliation and strongly deformed rocks. (c) Field photograph showing exfoliated and folding.

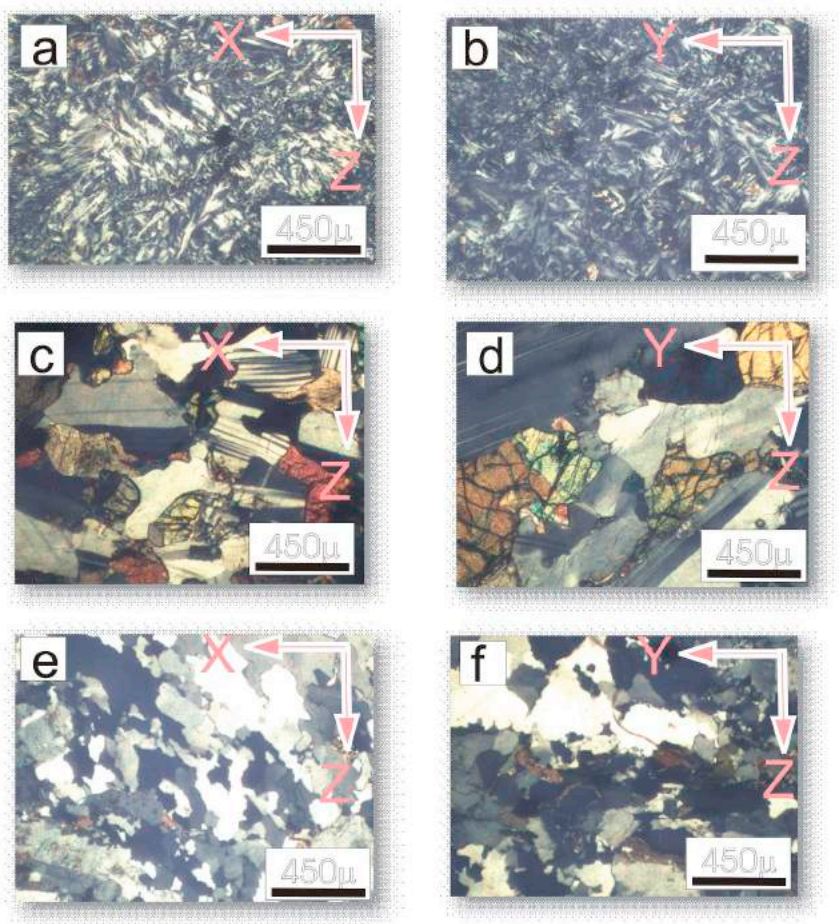

Fig. 4. (a) Well oriented clasts of serpentine rocks (Sample Z1a). (b) Some alteration for serpentine rocks into talc and carbonite grains (Sample Z3). (c) Elongated plagioclase grains for hornblende gabbro (Sample Z12a). (d) Olivine gabbro weakly to moderate deformed (Sample Z13a). (e) Quartz Monzodiorite show elongated quartz and feldspars grains (Sample Z7). (f) Weakly to moderate deformed (Sample Z7).

relationships and considerable as a part of calc-alkalic magmatic core to the Siham volcanic arc. Quartz veins and aplite dikes and veins of different trends dissect all the rock units in the study area. They are discontinuous and trend northeast, dip 80–90° southeast and cover an area of about 1.5 b y 4 km.

3. Methodology

In the present work, granitic, metavolcanic rocks and amphibole schist samples are used for finite strain measurements in Zalm area. Using felsic minerals (feldspar, quartz and plagioclase) and mafic

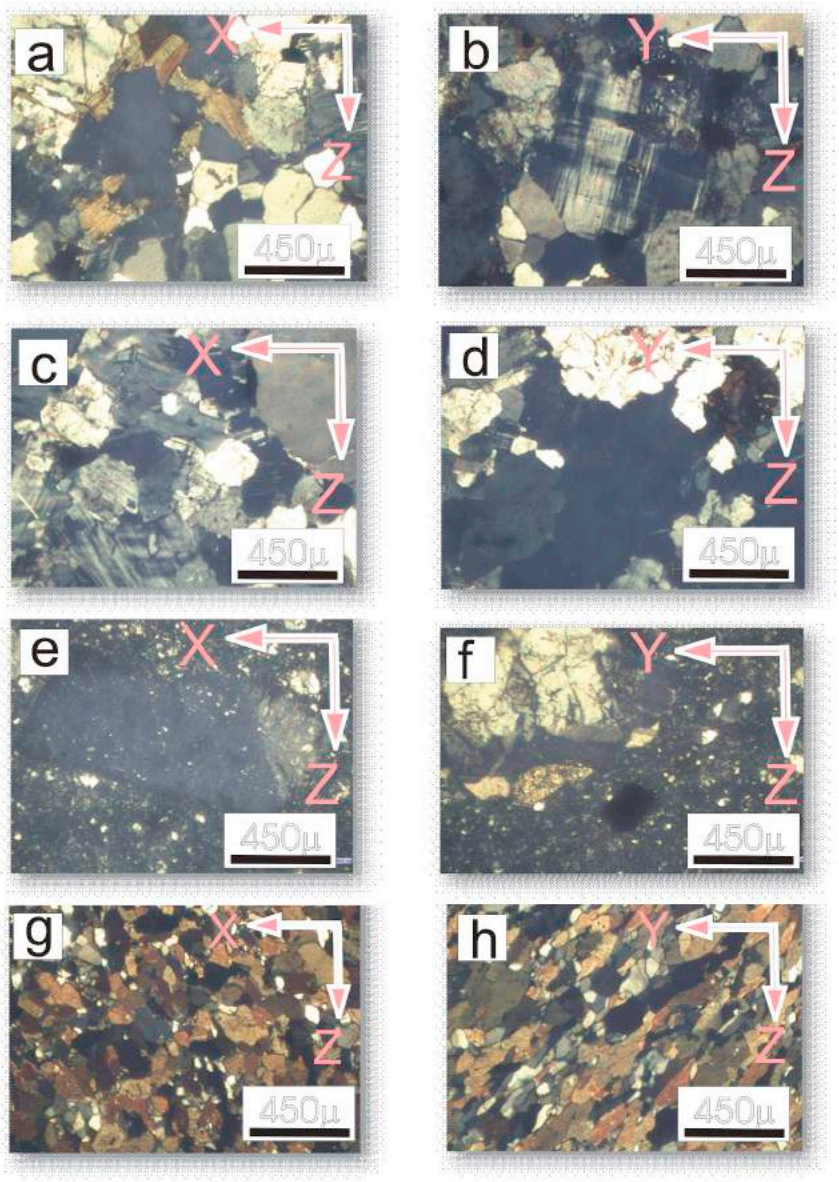

Fig. 5. (a) Weakly deformed for Alkali-feldspar granite (Sample Z10a). (b) Alkali-feldspar granite rocks composed of quartz, alkali-feldspar (orthoclase, perthite and microcline), muscovite (Sample Z11). (c) Course grains for Monzogranite rocks which consists of quartz, alkali-feldspar (orthoclase and perthite) and biotie minerals (Sample Z16a). (d) Elongated alkali-feldspars grains for Monzogranite rocks (Sample Z17). (e) Deformed rhyolite (meta-rhyolite) consists of quartz and alkali-feldspar (sanidine; Sample Z20a). (f) Metavolcanic rocks show elongated feldspars revealing moderate deformation (Sample Z20b). (g) Amphibole schist samples are moderately to highly deformed (Sample Z8a). (h) Amphibole schist with well oriented clasts of hornblende grains (Sample Z8c).

minerals (hornblende, biotite and chlorite) are measured by the R_f/ϕ and Fry methods (Fry, 1979; Ramsay, 1967; Ramsay and Huber, 1983). In order to estimate the three dimensional strain geometry ($X \geq Y \geq Z$, finite strain axes), we analyzed the two-dimensional strain which performed on XY, XZ and YZ sections. Two techniques in the present study (such as the R_f/ϕ and Fry methods) were used to check and estimate the finite strain data. The strain analysis which used fry technique represent the matrix strain, whereas the R_f/ϕ strains describe the clast strain (Ramsay and Huber, 1983; Ring, 1998). For R_f/ϕ analysis, the mean aspect ratio for each section was measured felsic minerals (feldspar, quartz and plagioclase) with some mafic minerals (hornblende, biotite and chlorite) through calculated the long and short axes per section. The measurement of the R_f/ϕ and fry methods should be cut the sample as thin sections along the XY, YZ and XZ sections and marked the felsic and mafic minerals. The traced outlines were then digitised. A least squares best-fit ellipse was calculated for each marker outline as well as its relative position and orientation. Peach and Lisle (1979) described that the chi-squared minima of the R_f/ϕ analyses were used to determine the tectonic strains. For fry analysis, the central points for feldspar, quartz and plagioclase grains per section (more than 100 grains) were used to calculate the strain analysis. We are used the modified least-square technique which are created by Owens (1984).

The magnitude of the Nadai strain is an important parameter, which is represented by an orthogonal coordinate system. It measured the natural principal strains E_X, E_Y and E_Z. Brandon, M. (1995) suggested that the distance from the origin provides an invariant measure of the total strain magnitude (E_t), that represented two orthogonal components: volume (E_v) and deviatoric (E_d) strain. E_v and E_d are independent of the rotational component of deformation.

$$E_t = (E_d^2 + E_v^2)^{1/2}$$

Twenty one (21) samples representative of each rock type were collected in the field work and about 40 thin sections were cut. Samples were cut and prepared in the King AbdulAziz University, Earth Science laboratory, Jidda, Saudi Arabia (Fig. 2). Thin sections of representative samples from the Zalm area were examined using polarized microscope to find out the mineral composition and textures, and to clarify effects of deformation, alteration and metamorphic grade of these rocks. The collected samples include 6 granitoid, 4 gabbro, 4 serpentinite, 2 metagrainte and 5 schist samples. The R_f/ϕ and fry methods were used the quartz, feldspar and mafic grains to determine the strain in the deformed granitiod, metavolcanics and amphibole schist samples.

Table 1
Finite strain data for sample from Zalm area.

Samples No.	Methods	X	Y	Z	XY	YZ	XZ	K	r	LogX/Y	Log Z/Y	Nadi strain	Lode's
Z1a	Rf/Ø	1.3	1.24	0.62	1.05	2	2.09	0.04	2.05	0.02	−0.3	0.585	0.881
	Fry	1.2	1.06	0.79	1.13	1.35	1.52	0.38	1.48	0.05	−0.13	0.306	0.414
Z1b	Rf/Ø	1.37	1.23	0.59	1.11	2.09	2.33	0.11	2.2	0.05	−0.32	0.651	0.73
	Fry	1.09	1.05	0.87	1.04	1.21	1.26	0.17	1.25	0.02	−0.08	0.175	0.69
Z3	Rf/Ø	1.56	1.39	0.46	1.12	3.01	3.37	0.06	3.13	0.05	−0.48	0.95	0.816
	Fry	1.19	1.05	0.8	1.13	1.32	1.5	0.41	1.46	0.05	−0.12	0.294	0.382
Z5	Rf/Ø	1.39	1.29	0.56	1.08	2.31	2.49	0.06	2.39	0.36	−0.717	0.428	0.833
	Fry	1.22	1.09	0.75	1.12	1.46	1.63	0.26	1.58	0.05	−0.16	0.362	0.544
Z7	Rf/Ø	1.25	1.13	0.71	1.1	1.6	1.76	0.17	1.7	0.04	−0.2	0.428	0.655
	Fry	1.39	1.21	0.59	1.15	2.05	2.35	0.14	2.2	0.06	−0.31	0.65	0.683
Z8a	Rf/Ø	1.26	1.24	0.64	1.02	1.93	1.96	0.02	1.95	0.01	−0.29	0.544	0.945
	Fry	1.29	1.03	0.76	1.25	1.36	1.7	0.71	1.61	0.1	−0.13	0.375	0.152
Z8b	Rf/Ø	1.43	1.19	0.59	1.2	2.03	2.44	0.2	2.23	0.08	−31	0.666	0.582
	Fry	1.24	1.19	0.68	1.05	1.75	1.83	0.07	1.8	0.02	−0.24	0.476	0.843
Z8c	Rf/Ø	1.37	1.2	0.61	1.14	1.99	2.27	0.14	2.13	0.06	−0.3	0.622	0.682
	Fry	1.37	0.99	0.73	1.39	1.35	1.87	1.1	1.74	0.14	−0.13	0.443	0.041
Z8d	Rf/Ø	1.3	1.23	0.63	1.05	1.96	2.07	0.05	2.02	0.02	−0.29	0.573	0.859
	Fry	1.22	1.01	0.81	1.2	1.26	1.52	0.79	1.64	0.08	−0.1	0.294	0.105
Z8e	Rf/Ø	1.34	1.2	0.63	1.12	1.91	2.14	0.13	2.03	0.05	−0.28	0.581	0.702
	Fry	1.48	0.88	0.77	1.7	1.14	1.93	5.08	1.83	0.23	−0.06	0.492	0.609
Z10a	Rf/Ø	1.26	1.22	0.65	1.04	1.87	1.94	0.05	1.91	0.02	−0.27	0.527	0.883
	Fry	1.37	1.05	0.7	1.3	1.5	1.95	0.61	1.8	0.12	−0.17	0.475	0.204
Z10b	Rf/Ø	1.28	1.11	0.71	1.16	1.57	1.82	0.28	1.73	0.06	−0.19	0.439	0.505
	Fry	1.19	1.12	0.75	1.06	1.5	1.58	0.12	1.55	0.02	−0.17	0.354	0.751
Z11	Rf/Ø	1.23	1.15	0.71	1.07	1.63	1.75	0.11	1.7	0.03	−0.21	0.43	0.76
	Fry	1.28	1.03	0.76	1.25	1.35	1.69	0.71	1.6	0.1	−0.13	0.373	0.151
Z12a	Rf/Ø	1.27	1.22	0.64	1.04	1.9	1.98	0.05	1.94	0.02	−0.28	0.543	0.882
	Fry	1.29	1.28	0.61	1.01	2.11	2.13	0.01	2.12	0	−0.32	0.613	0.984
Z12b	Rf/Ø	1.24	1.21	0.67	1.02	1.82	1.86	0.03	1.84	0.01	−0.26	0.498	0.921
	Fry	1.29	1.28	0.61	1.01	2.11	2.13	0.01	2.12	0	−0.32	0.613	0.984
Z13a	Rf/Ø	1.24	1.21	0.66	1.02	1.82	1.87	0.03	1.85	0.01	−0.26	0.501	0.922
	Fry	1.29	1.28	0.61	1.01	2.11	2.13	0.01	2.12	0	−0.32	0.613	0.984
Z13b	Rf/Ø	1.24	1.2	0.67	1.04	1.79	1.85	0.05	1.82	0.02	−0.25	0.489	0.886
	Fry	153	1.01	0.65	1.52	1.56	2.37	0.92	2.08	0.18	−0.19	0.611	0.032
Z16a	Rf/Ø	1.25	1.23	0.65	1.02	1.9	1.93	0.02	1.91	0.01	−0.28	0.529	0.954
	Fry	1.28	1.11	0.7	1.15	1.59	1.84	0.26	1.74	0.06	−0.2	0.449	0.53
Z16b	Rf/Ø	1.24	1.22	0.66	1.02	1.84	1.87	0.02	1.86	0.01	−0.27	0.505	0.95
	Fry	1.31	1.06	0.72	1.23	1.48	1.81	0.48	1.7	0.09	−0.17	0.427	0.309
Z17	Rf/Ø	1.26	1.23	0.65	1.03	1.91	1.95	0.03	1.93	0.01	−0.28	0.537	0.926
	Fry	1.23	1.15	0.71	1.08	1.62	1.74	0.12	1.69	0.03	−0.21	0.425	0.735
Z20a	Rf/Ø	1.18	1.18	0.72	1.01	1.64	1.65	0.01	1.65	0	−0.21	0.406	0.976
	Fry	1.68	0.91	0.66	1.85	1.38	2.56	2.24	2.24	0.27	−0.14	0.676	0.313
Z20b	Rf/Ø	1.19	1.17	0.72	1.02	1.63	1.66	0.03	1.65	0.01	−0.21	0.407	0.928
	Fry	1.42	1.05	0.67	1.35	1.56	2.11	0.63	1.92	0.13	−0.19	0.532	0.19

4. Microstructure and deformation

In the present work, microstructural and deformation were investigated by using thin sections. The prepared thin sections cut normal to the foliation and parallel to the lineation (XZ), normal to the foliation and lineation (YZ) and parallel to the foliation (XY). The investigated samples are displayed by ESE-WNW and N−S direction with low to moderate dip. The foliation shows the northeast-southwest and east-west direction with shallow plunge in the different deformed rocks such as amphibolite schist, granitoid, metavolcanic, serpentinite and gabbroic rocks. In addition, the lineation have a trend NW-SE and W-E with shallow dip.

The amphibolites are characterized by a conspicuous schistosity resulted from subparallel alignment of hornblende, plagioclase and biotite. The amphibolites are thrusted the granitoid rocks (Fig. 3a). They are sheared, brecciated, cataclased and occasionally partly migmatized (Fig. 3b). The sheared granites outcrop in several locations in the mapped area. They are jointed and intruded by mafic dykes dipping toward eastward (Fig. 3a). They are exfoliated and include xenolithic enclaves, which were foreign bodies captured from the surrounding country rocks by the igneous protolith of the granitoids. The contacts between the granitoids and surrounding lithologies are intensively sheared and have subvertical foliations. The banding and foliation were deformed by folding (Fig. 3c).

Serpentinite samples in the Zalm area consist of serpentine, talc and carbonite. The vertical foliation defined by low to moderate deformation has been observed in the serpentinite with well oriented clasts of serpentine, talc and carbonite grains (Fig. 4a and b). Gabbro does not shown deformation. Gabbro rocks consist of plagioclase and mafic minerals such as clinopyroxene, orthopyroxene and olivine (Fig. 4c and d). The gabbroic rock complex of the study area can be distinguish petrographically into two main types. The first type is hornblende gabbro consisting of plagioclase, clinopyroxene, orthopyroxene, and hornblendic amphibole (Fig. 4c), and the second is Olivine gabbro consisting mainly of plagioclase, clinopyroxene, orthopyroxene (hypersthine) and olivine (Fig. 4d).

The granitoid rocks in the Zalm area, are divided into Quartz Monzodiorite, Alkali-feldspar, and Monzogranite. Granitiod rocks show elongated few quartz, feldspars grains and plagioclase weakly deformed. The Quartz Monzodiorite contains of quartz, plagioclase, alkali-feldspar (orthoclase, perthite and microcline) and some mafic minerals (such as biotite and hornblende) (Figs. 4e and 5f). Alkali-feldspar granite consists of alkali-feldspar minerals (such as orthoclase, perthite and microcline), quartz, muscovite and biotite (Fig. 5a and b). Monzogranite contains quartz, alkali-feldspar minerals (orthoclase and perthite), hornblende and biotite (Fig. 5c and d).

Deformed rhyolite (meta-rhyolite) consists of quartz and alkali-feldspar (sanidine). Elongated feldspars revealing moderate

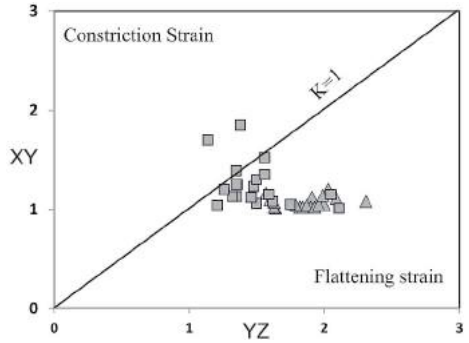

Fig. 6. Flinn diagram (Flinn, 1962) showing relative strain symmetry obtained from R_f/φ method (grey triangle) and fry method (grey square).

deformation and elongated quartz grains have also been observed in the Zalm area (Fig. 5e). It is absorved that the metavolcanic samples are weakly deformed (Fig. 5f) with elongated feldspars and quartz grains. In some places, the metavolcanic rocks display an elongated texture.

The schist samples are moderate to highly deformed (Fig. 5g and h). The vertical foliation defined by high to moderate deformation has been observed in the amphibole schist with well oriented clasts of hornblende grains (Fig. 5g and h). Schist samples consist of hornblende and quartz in the Zalm area. In other case, some grains of quartz are elongated and rotated. In addition, the Zalm area is characterized by the occurrence of gold and chromite mineralization. The chromite exists in the ultramafic rocks, whereas the gold is associated with quartz veins intruding along shear zones.

5. Strain measurements

The strain data are summarized in Table 1 and Figs. 5–9. The axial ratios of the Rf/ϕ and Fry methods in the XZ sections range from 1.65 to 3.37 and 1.26 to 2.56 respectively for the Schist, metavolcanics and deformed granitiods rocks (see Table 1). The axial ratios in the YZ sections range from 1.57 to 3.01 for the Rf/φ method and 1.14 to 2.11 for Fry method for the Schist, metavolcanics and deformed granitiods rocks (Table 1). The axial ratios of the Rf/ϕ method in the XY sections range from 1.57 to 3.01. Furthermore, the axial ratios of the Fry method in the XY sections range from 1.14 to 2.11 for the Schist, metavolcanics and granitiods rocks (Table 1).

Finite strenches indicate a narrow range of deformation of the different type of rocks. In addition, the stretches in the X direction (S_X) range from 1.18 to 1.56 for the Rf/ϕ technique and from 1.09 to 1.53 for the Fry technique. The strain in the Y direction (S_Y) ranges from 1.11 to 1.39 for the Rf/ϕ method and from 0.88 to 1.28 for the Fry method that show both contraction and extension deformation. In the Z direction, the stretches (S_Z) range from 0.46 to 0.72 that indicate vertical shortening of 28%–54% for the Rf/ϕ technique. In Fry technique, S_Z ranges from 0.59 to 0.87, that display vertical shortening of 13%–41% (Table 1). The data show no significant difference in the deformation behavior between Rf/ϕ and Fry techniques. In other word, the deformation have same order in all studied rock types, which apparent in the field (Figs. 6–10).

The axial ratios of the Rf/ϕ and Fry techniques in the K sections range from 0.01 to 0.28 and 0.01 to 5.08 respectivity for the Schist, metavolcanics and granitiods rocks (Table 1). The axial ratios of the Rf/ϕ method in the Nadi strain sections range from 0.406 to 0.950 and 0.175 to 0.676 for fry method in the different type of rocks (Table 1). The axial ratios of the Rf/ϕ method in the Lode's sections range from 0.505 to 0.976 for the Schist, metavolcanics and granitiods rocks and variety from 0.032 to 0.984 for fry method in the same type of rocks (Table 1).

The related strain data are summarized in Table 1 and given in a Flinn diagram (Fig. 6), which divided into prolate and oblate shapes for the strain ellipsoids. Hossack (1968) classified the strain symmetry into constrictional vs flattening, which shows information on volumetric strain. However, we are expected minor or no volume changes, due to the porosities during deformation very slight, specially in the basement rocks (Kassem and Ring, 2004).

As shown in Figure (5), the Rf/ϕ strains display flattening and constrictional symmetry. In general, the majority of samples are in a zone of flattening symmetry, while a few samples are showing constrictional symmetry. The Fry strains reveal 19 samples with flattening symmetry and 3 samples fall constrictional symmetry. Hence, the Rf/ϕ values derived from the analysis of quartz, alkali-feldspar, plagioclase and some mafic minerals represent regional strains (Fig. 6).

The studied samples display that no major difference in deformation behavior for the feldspar, amphibole minerals, and the quartz-mica matrix are observed. In addition, the similar deformation for investigated samples was shown during the metamorphic conditions and characterized of the same magnitude. Thus, the main phase of foliation is comparable in Schist, metavolcanics, amphibolites and deformed granitiods samples, showing similar deformation behavior in all different types of rocks (Figs. 7 and 8).

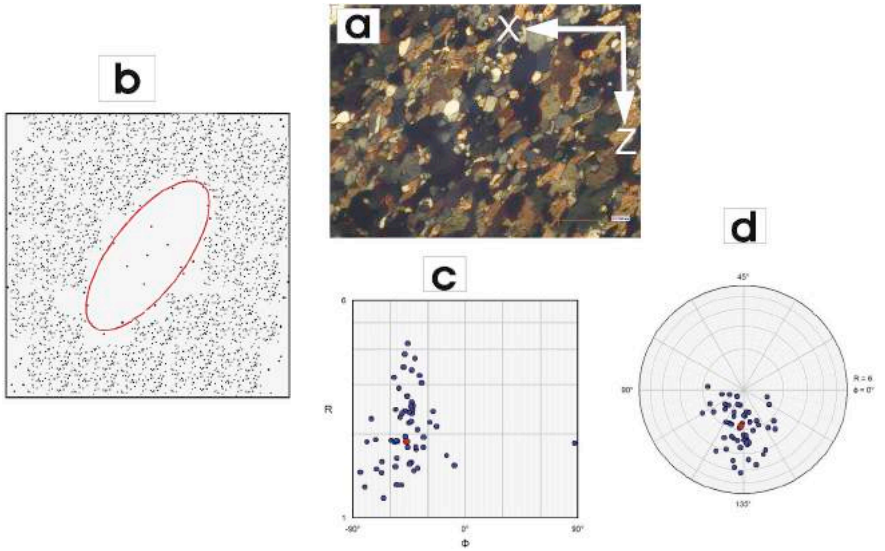

Fig. 7. a) Finite strain graph of XZ plane for Z8d sample, b) showing center to center graph, c) showing Rf/phi graph, d) showing polar graph.

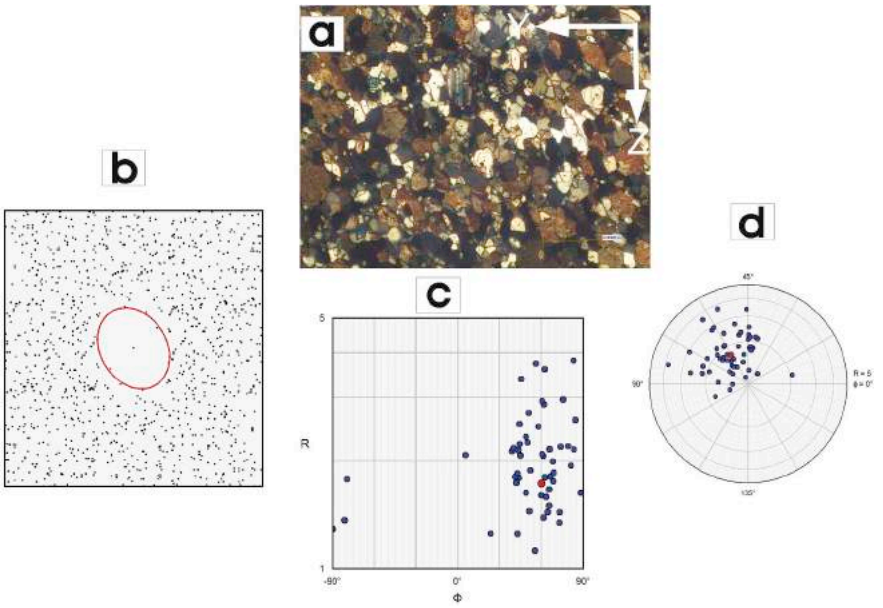

Fig. 8. a) Finite strain graph of YZ plane for Z8d sample, b) showing center to center graph, c) showing Rf/phi graph, d) showing polar graph.

The data shows relationship between the finite strain and strain axes in the Zalm area. The axial ratio between XZ vs YZ showing pronounced positive correlation (Fig. 9a). The axial ratio between XY vs XZ shows pronounced positive correlation (Fig. 9b). These characteristics indicate the prolate nature of the strain symmetry. The relationship between principal strain Ratios (K) vs Strain magnitude (ET) shows he data for Rf/ϕ less than Fry method, also the axial ratio between K vs (ET) displays pronounced more or less constant correlation (Fig. 10a). In addition, the relationship between Principal strain Ratios (K) vs Lode's parameter (LP) indicates that the data shows for Rf/ϕ less than Fry method, also the axial ratio between K vs (LP) shows pronounced negative correlation (Fig. 10b). The relationship between strain magnitude (ET) vs Lode's parameter (LP) showing the data for Rf/ϕ and Fry method mainly constant (Fig. 10c). The axial ratio between (ET) vs (LP) also shows pronounced randoum correlation for Rf/φ method, while the axial ratio between (ET) vs (LP) shows pronounced wide distribution correlation for Fry method (Fig. 10c).

6. Discussion

The Zalm ultramafic complex forms a segment of the Ad-Dafinah belt, which represented as part of the Nabitah suture zone (Stoeser and Camp, 1985). These ultramafic rocks display as scattered bodies near the Zalm area. It was intruded as a thick sill between the Lamisah shale and rhyolite member of the Bahjah Formation and now occupies the core of a northeast-trending downward facing antiform. It comprises talc schist and listwanite with many magnesite veins and a core of massive serpentinite that appears to be layered. The layering cannot directly be confirmed at the outcrop, although a base gabbronorite preserves primary igneous layering which is parallel to that inferred in the serpentinite and the bedding of the envelope. The gabbronorite is rhythmically layered with clinopyroxene at the base and labradorite/bytwonite at the top. Original petrographic features of the serpentinite are difficult to recognize but Sustrac (1980) reported the presence of dunite and pyroxene peridotite within the complex.

The tectonic evolution of the Zalm area seems to have undergone three main stages, namely Subducion, Nabitah orogeny and Najd orogeny. It is suggested that the Tamran Formation represents a part of the Jiddah terrane before the beginning of the Jiddah-Afif convergence. Shallow-marine continental-shelf sediments of the Siham Group have been deposited on the western margin of the Afif terrane during subduction. The Jidh calc-alkaline rocks are the product of subduction-related magmatism. The collision of Afif and Jiddah terranes coincided with the Nabitah orogeny, which was associated with folding and easterly directed overthrusting of the Siham Group, as well as syntectonic plutonism along the suture itself. The Najd orogeny began between about 640 and 630 Ma ago, following decline of the Nabitah orogeny. The unmetamorphosed volcanic and sedimentary rocks of the

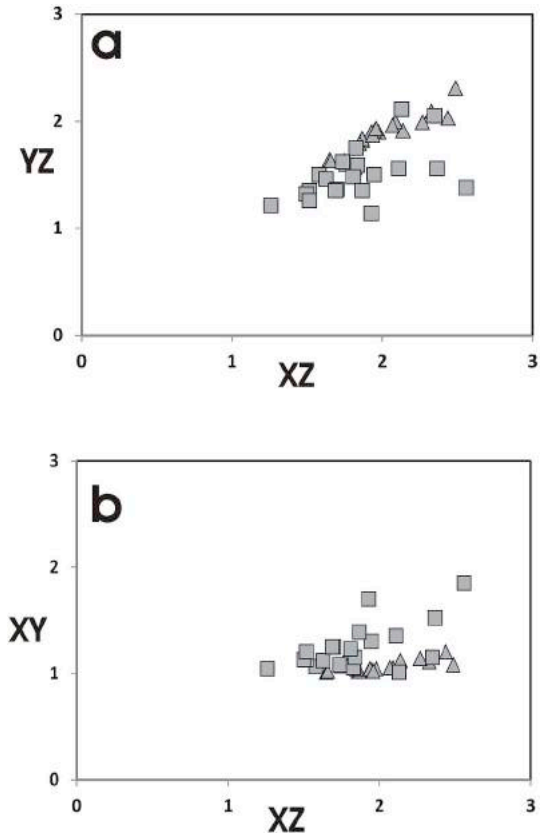

Fig. 9. The axial ratio showing the strain symmetry for the R_f/φ method (grey triangle) and Fry method (grey square). (a) The relation between YZ vs XZ (b) The relation between XY vs XZ.

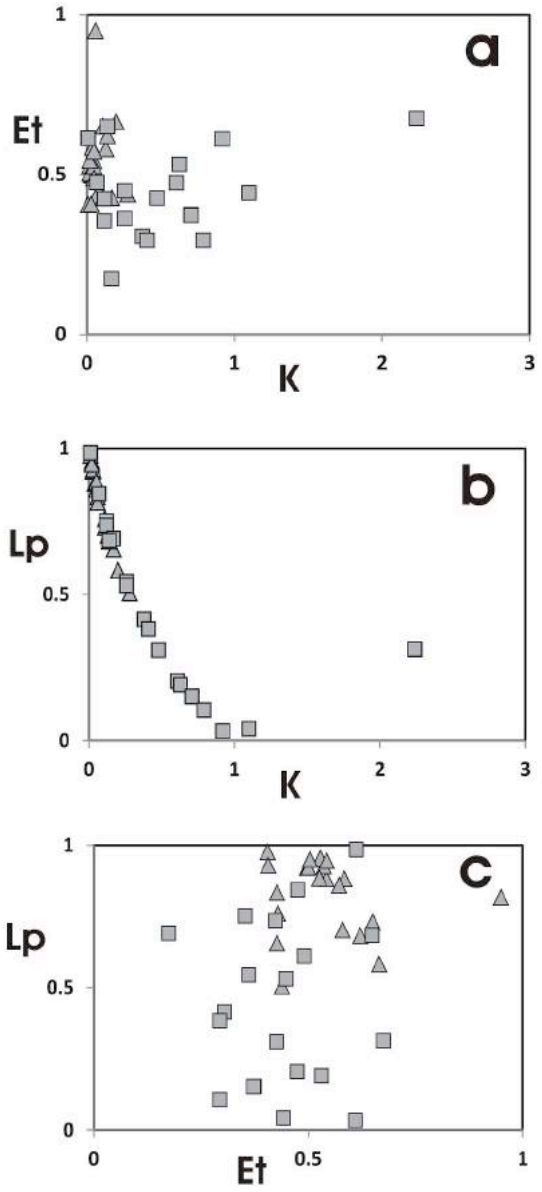

Fig. 10. Flinn diagram showing relative strain or strain symmetry as obtained by the R_f/φ method (grey triangle) and Fry method (grey square). (a) S_X vs K showing positive correlation. (b) S_Y vs K showing pronounced negative correlation. (c) S_Z vs K depicting no obvious correlation.

Bani Ghayy Group, exposed to the east of study area, were deposited in north-trending grabens that resulted from the transtension of the Najd strike-slip faulting. The structural framework created by the Najd orogeny has controlled the deposition of the Bani Ghayy Group and the early Phanerozoic rocks. However, Age dating for the different types of granitoid rocks is recommended to reveal their sequence of occurrence. Also detailed investigation of the unassigned ultramafic rocks will help for an adequate evaluating the gold mineralization in the Zalm area.

The Zalm area exhibits Neoproterozoic ultramafic-mafic rock complexes intruded by granitoid plutons. It contains; based on Johnson (2006); older Cryogenian layered rocks (Tamran Formation and Siham Group) and younger Cryogenian intrusive plutons (Jidh Suite and Humaymh Suite).

Our finite strain data shows that oblate strain symmetry (flattening strain) are observed in the Schist, metavolcanics, amphibolites and granitiods rocks of the Zalm area. The different lithology in the present area are displayed as flattening strain that indicate a general process causing flat-lying foliations. Our field work explain that granitiods rocks intruded the Schist and metavolcanics rocks. The strain magnitude are characterized by a wide-ranging and a heterogeneous deformation. On other word, the relationship between the strain magnitude and contacts does not detect (see Table 1). In addition, our strain magnitude data show the same order in the different lithology in the Zalm area. Therefore, we suggested that the Schist, metavolcanics and granitiods rocks have the similar deformation events at the same time approximately.

In the present work, the Rf/ϕ related strains created from ductile-deformed feldspar could be attributed to thrusting inspired deformation. Also, our data suggested that the deformation time for the accumulation of finite stain represents brittle to semi-ductile deformation during thrusting and intrusions of the deformed granitoids. It suggested that the structure and tectonic of the Zalm area is dominantly considered by pervasive and sub-horizontal foliations from the main metamorphic phase, which are almost sub parallel to the fault contacts in the Zalm area.

7. Conclusion

The investigations of strain and deformation data for the Zalm area are concluded as the following remarks:

- The strain data are characterized by both oblate strain and prolate strain symmetry in the Zalm area.
- This explains that the time of deformation is the accumulation of brittle to semi-ductile deformation during thrusting and intrusions.
- The accumulated of finite strain created during superimposed deformation. It explained that the contacts formed during the accumulation of finite strain.
- During thrusting the accumulation of brittle-semi-ductile deformation was not formed by simple shearing but the pure shearing is also important played due to a vertical shortening. It is concluded that the vertical shortening was effected by the sub-horizontal foliation in the studied area.
- It is suggested that the tectonic contacts were created during deformation and metamorphism with progressive over thrusting under brittle-semi-ductile conditions. In addition, the main-phase foliation is the same for Schist, metavolcanics, amphibolites and granitiods rocks, which also displays similar of deformation behavior in the different lithology.

Acknowledgements

The authors would like to extend their sincere appreciation to the Deanship of Scientific Research at King Saud University for its funding of this research through the Research Group project No. RG-1438-059.

References

Al-Shanti, A., Mitchell, A., 1976. Late precambrian subduction and collision in the Al Amar—Idsas region. Arabian Shield, Kingdom of Saudi Arabia: Tectonophysics 30 (3), T41–T47.
Altherr, R., Henjes-Kunst, F., Baumann, A., 1990. Asthenosphere versus lithosphere as possible sources for basaltic magmas erupted during formation of the Red Sea: constraints from Sr, Pb and Nd isotopes. Earth Planet Sci. Lett. 96, 269–286.
Camp, V.E., Roobol, J., 1992. Upwelling asthenosphere beneath western Arabia and its regional implications. J. Geophys. Res. 97 (B11) 15,255–15,271.
Coward, M.P., 1976. Strain within ductile shear zones. Tectonophysics 34, 184–197.
Flinn, D., 1962. On folding during three-dimensional progressive deformation. Q. J. Geol. Soc. Lond. 118, 385–433.
Fritz, H., Wallbrecher, E., Khudier, A.A., Abu El Ela, F., Dallmeyer, R.D., 1996. Formation of Neoproterozoic metamorphic core complexes during oblique convergence, eastern Desert, Egypt. J. Afr. Earth Sci. 23, 311–329.
Fry, N., 1979. Random point distributions and strain measurement in rocks. Tectonophysics 60 (1–2), 89–105.
Hansen, S.E., Rodgers, A.J., Schwartz, S.Y., Al-Amri, A.M.S., 2007. Imaging ruptured lithosphere beneath the red sea and Arabian peninsula. Earth Planet Sci. Lett. 259, 256–265.
Hossack, J.R., 1968. Pebble deformation and thrusting in the Bygdin area (Southern

Norway). Tectonophysics 5, 315–339.
Johnson, P.R., 2006. Explanatory Notes to the Map of Proterozoic Geology of Western Saudi Arabia. Saudi Geological Survey Technical Report SGS-TR-2006-4. 62 pp., Scale 1:1,500,000.
Johnson, P.R., Kattan, F.H., 2012. The geology of the Saudi Arabian shield. Saudi Geological Survey: Jiddah, Saudi Arabia 1–479.
Johnson, P.R., Abdelsalam, M.G., Stern, R.J., 2003. The Bi'r Umq-Nakasib suture zone in the Arabian-Nubian Shield: a key to understanding crustal growth in the East African Orogen. Gondwana Res. 6, 523–530.
Johnson, P.R., Kattan, F.K., Al-Saleh, A.M., 2004. Neoproterozoic ophiolites in the Arabian shield: field relations and structure. In: In: Kusky, T.M. (Ed.), Precambrian Ophiolites and Related Rocks, Developments in Precambrian Geology, vol. 13. Elsevier, pp. 129–162.
Johnson, P.R., Andresen, A., Collins, A.S., Fowler, A.R., Fritz, H., Ghebreab, W., Kusky, T., Stern, R.J., 2011. Late Cryogenian-Ediacaran history of the Arabian-Nubian Shield: a review of depositional, plutonic, structural, and tectonic events in the closing stages of the northern East African Orogen. J. Afr. Earth Sci. 61, 167–232.
Kassem, O.M.K., 2011. Determining heterogeneous deformation for granitic rocks in the northern thrust in Wadi Mubark belt, eastern desert, Egypt. Geotectonics Journal 45 (3), 244–254.
Kassem, O.M.K., 2012. Kinematic vorticity technique for porphyroclasts in the metamorphic rocks: an example from the northern thrust in Wadi Mubarak belt, eastern desert, Egypt. Arabian Journal of Geosciences 5 (1), 159–167.
Kassem, O.M.K., 2014. Kinematic analysis of the Migif area in the eastern desert of Egypt. J. Afr. Earth Sci. 90, 136–149.
Kassem, O.M.K., 2015. Strain analysis and deformation in the tanumah area, Arabian shield, Saudi Arabia. Arabian Journal of Geosciences 8 (6), 4127–4138.
Kassem, O.M.K., Abdel Raheim, S., 2010. Finite strain analysis for the metavolcanic-sedimentary rocks in the gabel El- Mayet region, central eastern desert, Egypt. J. Afr. Earth Sci. 58, 321–330.
Kassem, O.M.K., Ring, U., 2004. Underplating-related finite-strain patterns in the Gran Paradiso massif, Western Alps, Italy: heterogeneous ductile strain superimposed on a nappe stack. J. Geol. Soc. 161, 875–884 London.
Kassem, O.M.K., Abd El Rahim, S.H., El Nashar, E.R., 2012. Strain analysis and microstructural evolution characteristic of neoproterozoic rocks associations of Wadi El Falek, centre eastern desert, Egypt. Geotectonics 46 (5), 379–388.
Kassem, O.M.K., Abdullah, L.A. Almutairi, Al Bassam, Abdel Aziz M., Al Faifi, Hussain J., 2016. Relationship between finite Strain and tectonic setting in the Ar Ruwaydah area, eastern Arabian Shield, Saudi Arabia. Arabian Journal of Geosciences 9 (19:728), 1–10.
Mooney, W.D., Gettings, M.E., Blank, H.R., Healy, J.H., 1985. Saudi Arabian seismic-refraction profile; a traveltime interpretation of crustal and upper mantle structures. Tectonophysics 111, 173–246.
Mukul, M., Mitra, G., 1998. Finite strain and strain variation analysis in the sheeprock thrust sheet: an internal thrust sheet in the provo salient of the Sevier Fold-and –thrust belt, Central Utah. J. Struct. Geol. 20 (4), 385–405.
Neumayr, P., Mogessie, A., Hoinkes, G., Puhl, J., 1996. Geological Setting of the Meatiq metamorphic core complex in the Eastern Desert of Egypt based on amphibolite eochemistry. J. Afr. Earth Sci. 23, 331–345.
Neumayr, P., Hoinkes, G., Puhl, J., Mogessie, A., Khudier, A.A., 1998. The Meatiq dome (Eastern desert, Egypt) a Precambrian metamorphic core complex: petrological and geological evidence. J. Metamorph. Geol. 16, 259–279.
O´Hara, K., Blockburn, W.H., 1989. Volume-loss model for trace element enrichments in mylonites. Geology 17, 524–527.
Owens, W., 1984. The calculation of a best-fit ellipsoid from elliptical sections on arbitrarily orientated planes. J. Struct. Geol. 6 (5), 571–578.
Peach, C., Lisle, R.J., 1979. A Fortran IV program for the analysis of tectonic strain using deformed elliptical markers. Comput. Geosci. 5 (3), 325–334.
Ramsay, J., 1967. Folding and Fracturing of Rocks. McGraw-Hill Book Company, New York, pp. 560.
Ramsay, J., Huber, M., 1983. Strain Analysis, the Techniques of Modern Structural Geology, vol. 1 Academic Press, London Strain Analysis.
Ring, U., 1998. Exhumation of blue schists from Samos Island. Geological Society of Greece Bulletin 32, 97–104.
Ring, U., 1999. Volume loss, fluid flow, and coaxial vs non-coaxial deformation in retrograde, amphibolite-facies shear zones, northern Malawi, east-central Africa. Geol. Soc. Am. Bull. 111, 123–142.
Sandvol, E., Seber, D., Barazangi, M., Vernon, F.L., Mellors, R., Al-Amri, A., 1998. Lithospheric seismic velocity discon tinuities beneath the Arabian Shield. Geophys. Res. Lett. 25, 2873–2876.
Simpson, C., De Poar, D.G., 1993. Strain and Kinematic analysis in general shear zones. J. Struct. Geol. 15, 1–20.
Stern, R., 1985. The Najd Fault System, Saudi Arabia and Egypt: a ate Pre-cambrian rift-related transform system? Tectonics 4, 497–511.
Stern, R.J., Johnson, P.J., Kröner, A., Yibas, B., 2004. Neoproterozoic ophiolites of the Arabian–nubian shield. In: Kusky, T. (Ed.), Precambrian Ophiolites. Elsevier, Amsterdam, pp. 95–128.
Stoeser, D.B., Camp, V.E., 1985. Pan-African microplate accretion of the Arabian Shield. Geol. Soc. Am. Bull. 96 (7), 817–826.
Sustrac, G., 1980. Synthesis Report on the Basic and Ultrabasic Rocks of Saudi Arabia: French Bureau de Recherches Geologiques at Minieres Open-File Report JED-OR-80-8. 239 pp.